Multicolored Emission and Lasing in DCM-Adamantane Plasma Nanocomposite Optical Films

María Alcaire[1], Luis Cerdán[2], Fernando Lahoz Zamarro[3], Francisco J. Aparicio[1], Juan Carlos González[1], Francisco J. Ferrer[4], Ana Borras[1], Juan Pedro Espinós[1], Angel Barranco[1*]*

[1]Consejo Superior de Investigaciones Científicas, Instituto de Ciencia de Materiales de Sevilla (CSIC-Universidad de Sevilla) c/Américo Vespucio 49, 41092 Sevilla, Spain.

[2]Instituto de Química-Física Rocasolano (CSIC). c/ Serrano 119, 28006 Madrid, Spain.

[3]Departamento de Física, Instituto Universitario de Estudios Avanzados, Universidad de La Laguna, C/ Astrofísico Francisco Sanchez s/n, 38206 La Laguna. Santa Cruz de Tenerife, Spain.

[4]Centro Nacional de Aceleradores (Univ. Sevilla- CSIC) Av. Thomas A. Edison, 7, E-41092 Sevilla, Spain

KEYWORDS: DCM, luminescence, lasing, ASE, DFB, plasma polymer, remote plasma, plasma polymerization

ABSTRACT

We present a low-temperature versatile protocol for the fabrication of plasma nanocomposite thin films to act as tunable emitters and optical gain media. The films are obtained by the remote plasma-assisted deposition of a DCM 4-(dicyano-methylene)-2-methyl-6-(4-dimethylamino-styryl)-4H-pyran (DCM) laser dye alongside adamantane. The experimental parameters that determine the concentration of the dye in the films and their optical properties, including light absorption, the refractive index and luminescence, are evaluated. Amplified spontaneous emission (ASE) experiments in the DCM/adamantane nanocomposite waveguides show the improvement of the copolymerized nanocomposites' properties compared to films that were deposited with DCM films as the sole precursor. Moreover, 1D distributed feed-back (DFB) laser emission is demonstrated and characterized in some of the nanocomposite films that are studied. These results open new paths for the optimization of the optical and lasing film properties of plasma nanocomposite polymers, which can be straightforwardly integrated as active components in optoelectronic devices.

1. INTRODUCTION

Plasma nanoscience approaches are increasing the number of novel synthetic approaches of advanced materials with properties that are difficult to achieve by alternative procedures.[1,2] In recent studies, we introduced an original remote plasma-assisted vacuum deposition (RPAVD) process to fabricate highly luminescent polymeric thin films from functional organic solid precursors.[2-6] These organic precursors, which mostly included dye molecules, were sublimated in the afterglow region of a low-power microwave plasma. Solid thin films were produced where a high concentration of dye molecules remained intact within a matrix of molecular fragments of

the same dye that formed from interactions with the plasma discharge. These previous results demonstrated that the properties of these films can be adjusted by controlling the interactions of sublimated dye molecules with the boundary region of the plasma discharge through the deposition parameters. Currently, this method has been applied to prepare luminescent films, optical sensors and photonic sensing chips.[5-7] A clear advantage of the RPAVD technique is its compatibility with integrated optoelectronics and wafer-scale production.[5,6] Herein, we aim to improve the control of the optical properties of these plasma films and thus expand the application of this methodology to the development of laser gain media. In addition, we present the first results of the use of 4-(dicyano-methylene)-2-methyl-6-(4-dimethylamino-styryl)-4H-pyran (DCM) solid powder as a precursor in a plasma-assisted deposition process.

DCM is a luminescent dye that was developed by Webster et al. in the mid-1970s for the Eastman-Kodak company.[8] The objective of their work was to extend the tunable range of dye lasers into the red range of the visible spectrum. Later, the molecule attracted considerable interest in the research community and was commonly used in diluted solutions in commercially available tunable dye lasers. When DCM is dissolved in polar solvents as methanol, its spectral properties are characterized by a highly efficient and broad fluorescence and a relatively long excited-state lifetime.[9-11] DCM is an example of a donor-π-bridge-acceptor molecule that consists of an electron-donating dimethylamino group and an electron-accepting dicyano group that is separated by a conjugated bridge. This molecule undergoes a very fast intramolecular charge transfer (ICT) process under photoexcitation, which creates an ICT-excited state with a very high dipole moment (~ 26 D). This large dipole moment explains the strong solvatochromic shift of the reported fluorescent emission[12,13] of DCM in solution and as a dopant in organic solid hosts. This dye has been mainly studied and used in solution but has also been reported as a

dopant in organic light-emitting diodes,[14,15] solid state host-guest lasing systems,[16] and luminescent nanoparticles[17] and incorporated as pendant groups in fluorene copolymers.[18]

Adamantane precursor molecules consist of single C-C bonds with a relatively high vapor pressure at low temperatures (<50 ºC). Adamantane RPAVD films are highly transparent, presenting very low levels of plasma polymerization-induced conjugation (i.e., low absorption in the UV range) and thus lacking the typical yellowish color of hydrocarbon plasma polymers from absorption in the high-energy region of the visible spectrum.[3,4,19]

Amplified spontaneous emission (ASE) is a cooperative effect that occurs by the stimulated emission of radiation in a gain medium without requiring optical feedback. ASE is frequently used by researchers as a preliminary test to explore the suitability of organic materials for laser applications.[20-26] Moreover, optical feedback can be achieved in thin film devices without external mirrors, such as in distributed feedback (DFB) lasers. In these systems, the optical feedback is provided by Bragg scattering through periodic refractive index modulations in the film, the substrate, or both. In particular, one-dimensional (1D) DFB lasers have been successfully demonstrated in a variety of small-molecule systems (see 21, 22 and references therein) from different fabrication techniques, including dye-doped polymers. However, high dye concentrations are avoided for this type of application because dye fluorescence is very sensitive to concentration quenching.

This article is structured as follows. First, we demonstrate the fabrication of luminescent nanocomposite thin films, whereby integer DCM molecules are embedded within a transparent, insoluble, and thermally stable polymeric matrix. The structural, optical and luminescent

properties of the films are related to the deposition conditions. Second, we prove the application of DCM/adamantane nanocomposite films to the fabrication of a DFB laser.

2. EXPERIMENTAL SETUP

2.1 Materials

DCM (dye content 98%) and adamantane (>99%) powders were purchased from Sigma-Aldrich and used as received without further purifications. UV-transparent fused silica slides and doped and intrinsic Si(100) wafer pieces (both ~1x1 cm^2) were used as substrates.

2.2 Remote plasma-assisted vacuum deposition process

A complete description of the experimental setup for the deposition can be found elsewhere.[3,4,6] This system consisted of an electron cyclotron resonance (ECR) plasma reactor with two zones for the plasma and the remote deposition. In the plasma zone, an Argon microwave plasma (power: 150 W, pressure: 10^{-2} mbar) was sustained and confined through a set of magnets. Meanwhile, a low-temperature effusion cell in the deposition zone sublimated the dye onto the substrates, which were also placed in the afterglow of the plasma discharge. Additionally, a glass ampoule that contained adamantane powder was connected to the deposition chamber to supply a regulated vapor pressure of this compound into the deposition chamber. The sample holder consisted of a grounded metallic grid (~1 mm thick) between the effusion cell and the plasma zone. The substrates in this configuration were fixed to the bottom face of the sample holder, which faced the effusion cell. The distances between the sample holder and plasma zone (z) and between the effusion cell and the sample holder (d) were critical geometrical parameters that permitted us to regulate the interaction between the sublimated dye

and the plasma species and, therefore, the final material properties.[4,27] The film thickness and deposition rate (r) were monitored by using a quartz crystal microbalance (QCM) beside the sample holder. The registered values were corrected by a calibration factor from the thickness of the films, which was determined after deposition. The amount of precursor molecules that were dosed into the deposition zone, and therefore the deposition rate that was measured in the QCM, were regulated by adjusting the effusion cell and adamantane supply system's temperatures.

2.3 Thin film characterization

The surface chemical composition of the samples was analyzed by X-ray photoelectron spectroscopy (XPS) with an ESCALAB 210 spectrometer, which operated at a constant pass energy of 20 eV. Non-monochromatized Mg Kα radiation was used as the excitation source. The atomic surface concentrations were quantitatively determined from the areas of the C 1-s and O 1-s peaks. A Shirley-type background was subtracted, and the peak areas were corrected by the electron escape depth, the spectrometer transmission and the photoelectron cross-sections.[28]

Compositional measurements were obtained from proton elastic backscattering spectroscopy (p-EBS) for carbon, nitrogen and oxygen and by elastic recoil detection analysis (ERDA) for hydrogen. Elemental characterizations were performed at the 3-MV tandem accelerator of the National Center for Accelerators (Sevilla, Spain). EBS was performed with a proton beam of 2.0 MeV and a passivated implanted planar silicon (PIPS) detector at a 165º scattering angle. This energy was chosen to avoid interference from resonant cross sections of different elements in the samples and to clearly separate the signals from the light elements (C, N, and O) in the measured spectra. The advantages of this method have been described elsewhere.[29]-ERDA measurements were realized by using He ions with an energy of 3.0 MeV. The dispersion angle was 34º. A

collimator was placed in front of the detector to limit the detection to particles with this angle. A 13-μm-thick filter of aluminized Mylar was placed in front of the detector to prevent scattered He ions from arriving at the detector.

Fourier transform infrared (FTIR) spectra were collected in a JASCO FT/IR-6200 IRT-5000 under vacuum conditions and specular reflectance mode for layers that were deposited on gold-covered silicon wafers.

The surface topography of the films was studied by noncontact atomic force microscopy (AFM) with a Cervantes AFM system from NANOTEC and by using commercial noncontact AFM tips from MikroMasch.

The thermal stability of the films was analyzed in a tubular oven in a vacuum (10^{-2}-10^{-3} mbar) by heating the samples at 150 °C over 1 h. Solubility tests were conducted in water and toluene over 2 h at 25 ºC. After each immersion test, the films were dried in flowing nitrogen over 1 h at room temperature.

UV-Vis transmission spectra were acquired in a Varian Cary 300 spectrophotometer. The optical properties of the thin films were also studied with a variable angle spectroscopic ellipsometer (VASE) from J.A. Woollam Co., Inc. Depolarization measurements were performed at three incidence angles: 60°, 65°, and 70°. Transmission and depolarization data were analyzed by assuming the Cauchy dispersion law and an ensemble of three Lorentz oscillators. The thickness of the films was measured with a Mahr Surf XR-20 profilometer, and the obtained values were confirmed by ellipsometry.

Fluorescence spectra were recorded in a Horiba Jobin-Yvon Fluorolog-3 spectrofluorometer that operated in the front face mode. The emission spectra were excited with a radiation of 475 nm. Slits of 1- and 3-nm spectral width were used for the excitation and emission monochromators to obtain the emission spectra, respectively. The excitation spectra were obtained by using slits of 1.5 and 5 nm. The maxima of the excitation and emission bands were determined from uncorrected spectra. However, the position of the excitation maximum for sample DCM-ADA-6 was calculated after subtracting a spline baseline. The external radiative quantum efficiency of the films (η), which is defined as the ratio between the number of emitted photons and the number of photons that are absorbed by the film, was determined by an absolute method. The configuration consisted of a Labsphere, whose inner face was coated with Spectralon and attached to the spectrofluorometer. Spectral correction curves for the sphere and emission detector were provided by Horiba Jobin-Yvon. Time-resolved fluorescence decays were collected by using the time-correlated single-photon counting (TCSPC) option on the Fluorolog-3. A NanoLED350 that illuminated at 475 nm with a repetition rate of 1 MHz and a full width at half maximum of 1 ns was used to excite the sample. The signals were recorded by using an IBH Data Station Hub photon counting module, and data analysis was performed by using the commercially available DAS6 software (HORIBA Jobin-Yvon IBH). The fitting quality was assessed by minimizing the reduced chi squared function ($\chi_R^2 < 1.2$) and confirmed by the Durbin Watson parameter (DW > 1.7), visual inspection of the weighted residuals and autocorrelation of the residuals.

An optical parametric oscillator (OPO) pulsed laser that was tuned at 475 nm (10-ns pulse duration and 10-Hz repetition rate) was used as the excitation source for the ASE and DFB laser experiments. A pinhole was used to select a homogenous excitation laser beam. The OPO laser

output had horizontal polarization, so a λ/2 plate was used to induce vertical polarization. Two linear polarizers were used to modulate the intensity of the pump beam. The incident light on the sample was perpendicular to the film surface for both the ASE and laser measurements. For the ASE measurements, a cylindrical lens system focused the pump beam on the waveguide to form a horizontal line that was 10 mm long and 300 μm wide with an end placed at the edge of the film. For the DFB laser emission measurements, the pump beam was focused by using a spherical lens (focal length: 10 cm), and the sample was placed slightly out of the focus plane so that the excitation area of the pump beam was approximately 1 mm^2. Thus, a relatively large number of grooves were assured to contribute to the DFB laser oscillation. A long-pass filter was placed behind the sample to stop the pump beam. The edge ASE and the normal to the film DFB laser emission were collected with a 400-μm-diameter fiber-coupled CCD spectrometer (Andor, 0.1-nm resolution). Both the sample and the detection fiber were placed in micrometer translation stages.

For the DFB laser experiments, the thin films were deposited onto a 1.2 × 1.2-cm^2 quartz substrate that was engraved with a sinusoidal 1D grating with a period Λ = 377 nm and depth 100 nm (kindly provided by Dr. G. A. Turnbull, SUPA School of Physics & Astronomy, University of St. Andrews, UK). The grating area was centered on the quartz substrate and occupied a circular region of ~5 mm in diameter. The grating was fabricated by recording the required pattern on a spin-coated photoresist by means of interference lithography and subsequent attack with Reactive Ion Bean Etching (RIBE) to transfer the recorded pattern to the quartz substrate. The pattern was formed with a holographic setup in which two beams from a CW He-Cd laser were forced to interfere at a given angle θ and over a given time on the surface

of the photoresist. This two-beam interference created a 1D fringe pattern with a period $\Lambda = \lambda / (2\sin(\theta/2))$, where λ is the wavelength of the interfering beams.

3. RESULTS AND DISCUSSION

A set of thin DCM plasma polymer films was grown by varying the deposition conditions as summarized in Table 1. The main goal of this study was the dry synthesis of insoluble and thermally stable plasma polymeric films with a controllable amount of non-fragmented luminescent DCM molecules. This goal was accomplished by adjusting different experimental parameters to regulate the fragmentation of precursor molecules during the deposition and incorporation of the dye molecules into the growing film. As mentioned above, increasing the distance *z* between the substrates and the discharge is an efficient way to increase the concentration of these integer dye molecules in the films for given plasma conditions (i.e., power, pressure of gas, etc.). On the contrary, increasing the distance d_c between the sample holder and the effusion cell is an effective way to favor precursor fragmentation by interaction with the plasma species.[3,4,6] For given plasma deposition conditions, the percentage of dye molecules that remain intact during the deposition increases with the deposition rate.[3] Additionally, for the simultaneous remote plasma deposition of two different precursors, the relative presence of each precursor during the deposition process is evaluated through the ratio of the corresponding associated deposition rates.[4] Importantly, adamantane was introduced as a vapor in the reaction chamber, yielding highly cross-linked adamantane plasma polymers in all the surfaces that contacted the plasma (i.e., reactor walls and sample holder). On the contrary, DCM-containing films were only produced in the area of the sample holder in front of the organic evaporator cell. For the co-deposited DCM-ADA films, the deposition rate that was associated with adamantane was monitored from the quartz crystal monitor that closed the DCM

sublimation cell over short periods. The deposition rate that was associated with the sublimation of DCM was also roughly estimated from this value. Thus, the experimental conditions in the table were selected to gradually decrease the concentration of integer dye molecules from sample DCM-ADA-1 to DCM-ADA-6 as a function of d_c for a fixed z =10.5 cm. The deposition conditions in this work were directly selected from the final application of the synthesized films as optical/luminescent materials. Thus, a relatively low plasma power of 150 W and a working pressure of 10^{-2} mbar were kept fixed during all the experiments.

Table 1. DCM plasma polymer experimental growth conditions, including the distance between the effusion cell and sample holder and the ADA/DCM sublimation ratio as determined from QCM readings.

Sample	d_c (cm)	ADA/DCM sublimation ratio (a.u.)
DCM	7.0	0
DCM-ADA-1	5.8	1.0
DCM-ADA-2	5.8	1.5
DCM-ADA-3	5.8	2.0
DCM-ADA-4	5.8	4.0
DCM-ADA-5	11.6	2.0
DCM-ADA-6	11.6	4.0

3.1 Thin film composition and microstructure

The XPS analyses of the DCM-ADA film series indicated that the thin films' surfaces consisted of C, N and O depending of the deposition conditions, as expected given the composition of the precursors, namely, adamantane ($C_{10}H_{16}$) and DCM ($C_{19}H_{17}N_3O$). The calculated surface atomic ratios are shown in Table 2. In the first approach, the shape of the C 1-s, N 1-s and O 1-s core level spectra for the atomic percentage calculation were similar (spectra not shown), differing

only in their respective intensities. All the samples, including the ADA films, exhibited a relatively important percentage of oxygen in their composition. Thus, the DCM and DCM-ADA films were enriched in oxygen with respect to the percentage for the DCM stoichiometry, although the films were co-deposited with adamantane.

Table 2. XPS surface atomic ratios from the XPS analysis of a selected set of films.

	Ref. DCM-Sub.*	DCM	DCM-ADA-1	DCM-ADA-2	DCM-ADA-4	DCM-ADA-6	ADA
C 1 s (%at.)	79.4	74.0	82.5	87.1	88.2	88.3	88.3
O 1 s (%at.)	7.9	15.7	15.0	10.2	10.8	11.7	11.7
N 1 s (%at.)	12.7	10.3	2.5	2.7	1.0	0	0
N/C ratio	0.16	0.14	0.03	0.03	0.01	0	0
O/C ratio	0.10	0.21	0.18	0.12	0.12	0.13	0.13

*The atomic ratios that correspond to the DCM dye are C=82.6%, N=13.0%, O=4.0%, N/C=0.16 and O/C=0.05. The H content was not accessible by XPS.

The incorporation of oxygen in the films is a general characteristic of plasma processes originating from oxygenated species in the reactor and, in some cases, post-deposition reactions with the atmosphere.[30-32] The DCM-ADA films series presented a similar percentage of oxygen in their composition that was very close to the value of ADA films. These values were around two times the oxygen content in the DCM molecules, indicating that the precursor was not the main source of oxygen in the plasma films. This percentage was even higher in the plasma-polymerized DCM (DCM sample). The presence of a percentage of O around two times that of the dye composition in the sublimated films was very likely caused by moisture absorption and/or the surface oxidation of the dye crystallites. As the dye percentage in the DCM-ADA film series decreased from sample 1 to 6, the N atomic ratio decreased while the O content remained constant (O/C ratios ~ 0.12 in all cases but one). At higher dilution (DCM-ADA-6), the N signal

was not observable by XPS and the composition was identical to the ADA film. No N signal was observed in the ADA films, indicating that the dye was the only source of nitrogen in this system.

Bulk compositional measurements were performed by p-EBS for carbon, nitrogen and oxygen and ERDA to determine the hydrogen content in the samples. In this case, the results that correspond to the sublimated DCM reference samples were not available because of sample instabilities under ion bombardment fluxes during the p-EBS characterization. The results of this study are listed in Table 3.

Table 3. Thin films' bulk elemental compositions as determined by p-EBS and ERDA.

	DCM*	**DCM-ADA-2**	**DCM-ADA-4**	**DCM-ADA-6**	**ADA***
C (%at.)	45.0	47.0	45.0	46.0	43.0
N (%at.)	7.0	3.0	2.0	0.5	0
O (%at.)	3.0	2.0	2.5	1.5	3.0
H (%at.)	45.0	48.0	50.5	52.0	54.0
N/C ratio	0.16	0.06	0.04	0.01	0
O/C ratio	0.06	0.04	0.05	0.03	0.07

*Nominal atomic ratios for a) DCM: C=47.5%, N=7.5%, O=2.5%, H=42.5%, N/C=0.16, and O/C=0.05; and b) adamantane: C=38.5% and H=61.5%.

In all the samples, the O/C ratio was ~1/2 of the corresponding XPS value (Table 2), including the ADA film. The N/C values gradually decreased from 0.16 in the DCM film (a similar value to that of the DCM molecule) to 0.06 in the DCM-ADA-1 film, reaching a value of 0.01 in the DCM-ADA-6 film as the dilution of the dye increased. In addition, the films were gradually enriched in H as the ADA percentages in the films increased.

A comparison between the surface and bulk analyses indicated that a) the surfaces of the films were likely enriched in oxygen because of post-deposition reactions and plasma surface oxidation during the last stages of the films' deposition and b) the N content along the surface and within the volume could be a direct indicator of the dilution degree of the dye in the organic matrices. The N content was likely higher in the bulk than along the surface because of the same oxidation processes as mentioned above.

The FT-IR spectra of selected DCM and DCM-ADA films are shown in Figure 1. The IR features in the figure were determined according to the literature.[33] The spectra of the ADA RPAVD film and a sublimated DCM sample were included for comparison. The latter resembled the FT-IR spectrum that has been reported for this compound elsewhere.[34] The spectrum was dominated by a set of bands in the 1670-1500 cm^{-1} region, which corresponds to the different C=C and ring vibration modes of the molecule. Other relevant bands included the C-N stretching and the asymmetric and symmetric CH_3 deformation vibrations of the dimethylamino group at ~ 1370, 1440 and 1430 cm^{-1} respectively, and the C≡N stretching of the cyano group at ~ 2200 cm^{-1}. These spectra indicate other features that are related to different C-H vibration modes at $1/\lambda <$ 1300 cm^{-1} and within the 3100-2800 cm^{-1} region. The FT-IR spectrum of the RPAVD DCM film reproduced most of the bands in the spectrum of the sublimated sample but slightly broader and shifted. These structural characteristics are expected for films that consist of fragments from the partial breaking of the precursor and entire dye molecules. A comparison of the RPAVD and sublimated samples also revealed some structural changes from the plasma polymerization process. For instance, an important increase in the relative intensity of the features at $1/\lambda >$ 1640 cm^{-1}, which corresponds to C=C and/or C=O vibrations in acyclic structures, was clearly

apparent in the plasma polymer sample. This evolution was tentatively related to the breaking of the ring structures of the original precursor by the interaction with the plasma discharge.

Using adamantane as an additional precursor completely modified the structural characteristics of the films, as illustrated in Figure 1b. This figure clearly shows that the DCM-ADA films mainly consisted of a plasma polymeric matrix with similar structural characteristics to the ADA plasma polymer film. The most intense features in these spectra were the bands in the 3000-2800 cm^{-1} region, which were assigned to C-H_x stretching modes in aliphatic structures. Nevertheless, the DCM-ADA spectra indicated other vibrations that were associated with the dye molecules. The intensity of these bands decreased with the DCM concentration (cf. UV-Vis analyses in Figure 2) from sample DCM-ADA-2 to DCM-ADA-6. An easily identifiable example is the low-intensity C≡N stretching band at ~ 2200 cm^{-1}, which vanished in DCM-ADA-6's spectrum. These results illustrate the potential of the deposition methodology to control the structural characteristics of plasma polymer matrices with dye molecules.

Additional structural information regarding the films from the ToF-SIMS analyses is summarized in the Supporting information (S1). The results of this study are congruent with the XPS, RBS and FT-IR characterizations.

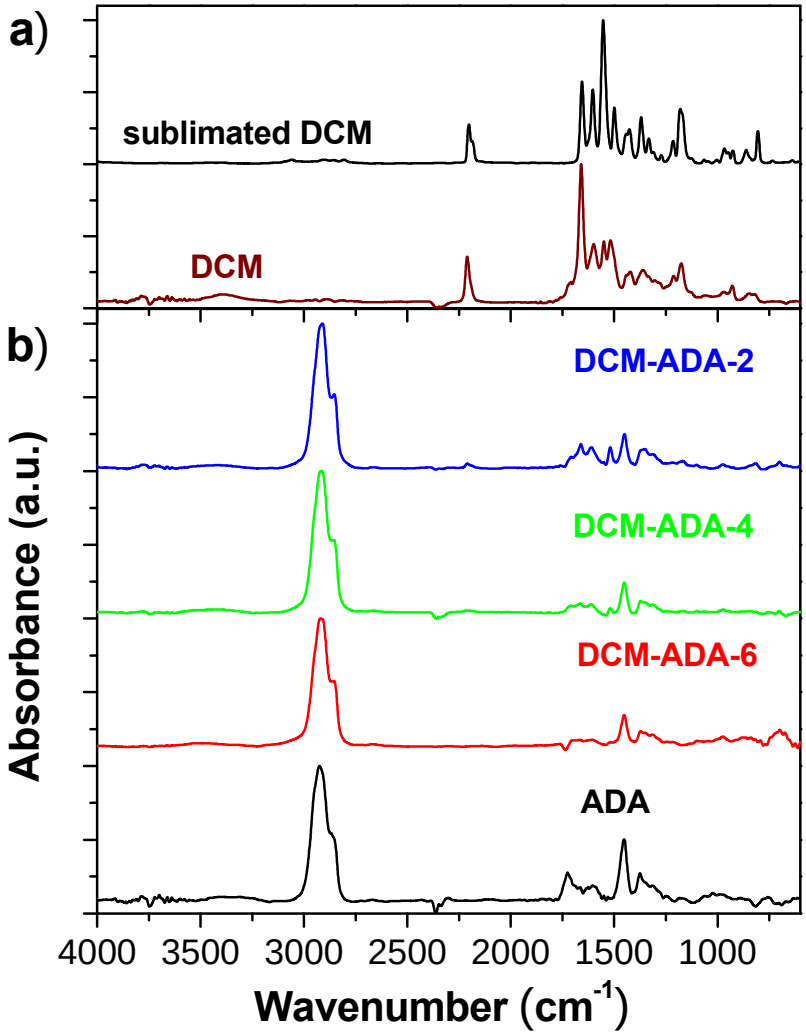

Figure 1. (a) FT-IR spectra of a DCM RPAVD film and a reference sublimated DCM sample. (b) FT-IR spectra of DCM-ADA films and a reference ADA film that was deposited by RPAVD.

The surface topography and roughness of the films were studied by AFM. The results indicated that the films were smooth, with RMS values lower than 0.6 nm for films in the range of 70-700 nm. These values were independent from the films' composition (from the ADA and DCM films to the DCM-ADA film series). The very low RMS values, the absence of defects as voids and

particles and their invariance with the films' thickness and composition are characteristics of the remote plasma-assisted vacuum deposition process.[3-7]

3.2 Optical properties

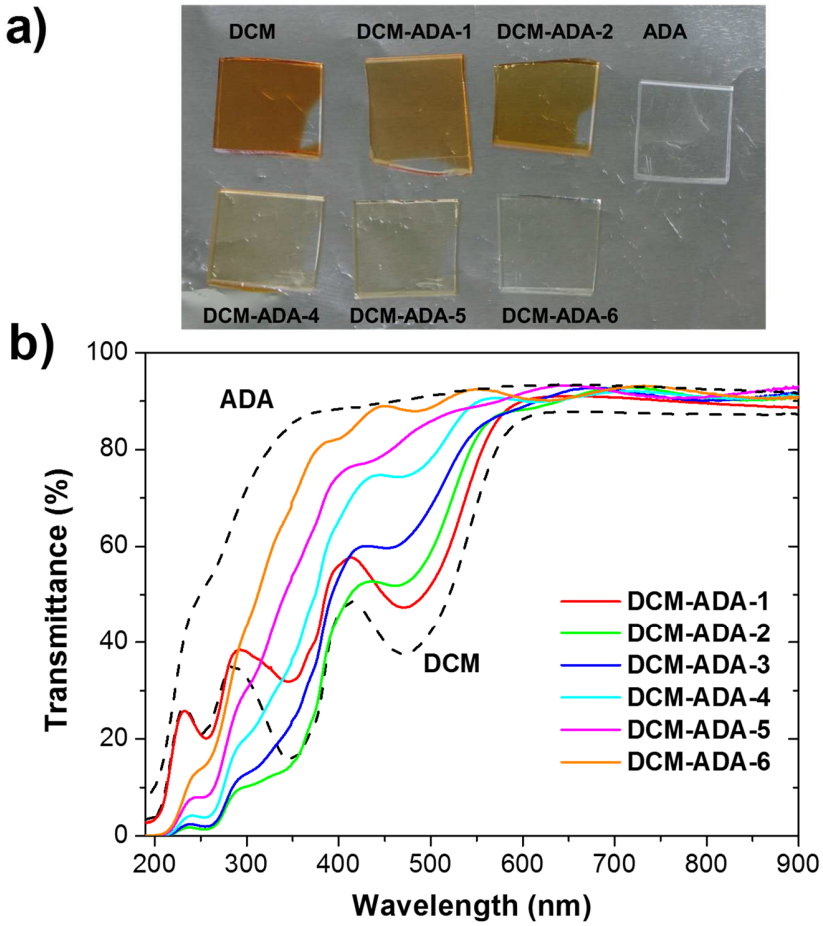

Figure 2. (a) Picture of DCM-ADA, DCM and ADA films that were deposited on fused silica substrates. (b) UV-Vis transmission spectra of the DCM-ADA series films, DCM films and ADA films.

Figure 2a and b show a picture and the transmittance spectra of a set of films that were deposited on fused silica substrates. The DCM-ADA plasma films had a similar thickness of ~650 nm, except for samples DCM-1 and DCM, which had a lower thickness (~200 nm) to avoid the saturation of the spectra. The films presented a similar red-orange coloration with different intensities depending on the deposition conditions, which directly indicates the presence of a percentage of integer dye molecules in their structures. These absorptions gradually decreased as a function of the dilution degree of the DCM dye in the films from sample DCM-ADA-1 to DCM-ADA-6. Thus, the more intense coloration corresponded to the DCM sample, whereas the ADA sample was completely transparent at wavelengths higher than ~300 nm. The DCM plasma film presented characteristic absorption features of the DCM dye at 475, 350 and 252 nm, which can be observed in the dye solutions or dispersions in polymers.[9-13] These characteristic absorptions, especially the 475 nm band, could be observed in the DCM-ADA plasma films but gradually decreased in intensity from sample DCM-ADA-1 to DCM-ADA-4, becoming very weak in sample DCM-ADA-5.

The DCM-ADA films also presented continuous absorption at wavelengths below 400 nm. This absorption could be attributed to the presence of unsaturated bonds in the film structure from the fragmentation, recombination and condensation of the sublimated DCM and adamantane precursor molecules during the films' growth because of their interaction with the plasma species. Such absorption is a general characteristic of plasma polymer films, including those that are deposited from saturated monomers[19,30,35], and is inherent to the formation of a solid cross-linked structure. For instance, this feature could be observed in the ADA film transmission curve at wavelengths below ~300 nm. Additionally, these films showed interference fringes in the

transparent region (λ> 600 nm) and in the 350-900 nm region, whereas the absorption at 475 nm was very weak (samples DCM-ADA-5 and 6).

Figure 3 shows the refractive index curves from the spectroscopic ellipsometry. The refractive index decreased as the DCM concentration in the film's composition decreased. This effect is related to the reduction of aromatic and unsaturated bond structures in the films.[3,4] Thus, the curve that corresponds to the DCM-ADA-6 film (n= 1.56 at 600 nm) is very close to that of plasma polymerized adamantane (n=1.55 at 600 nm), whereas the DCM-ADA-1 sample, which had the highest DCM content, had a refractive index of 1.66 at 600 nm. The refractive indices were relatively high compared to organic and polymeric films that are prepared by different techniques[3,5] Although the films absorbed in the visible range for wavelengths lower than 600 nm, the high refractive indices in the region around 600 nm, where the DCM dye fluoresces, are very relevant in terms of their integration in optoelectronic devices, which is shown in the next section.

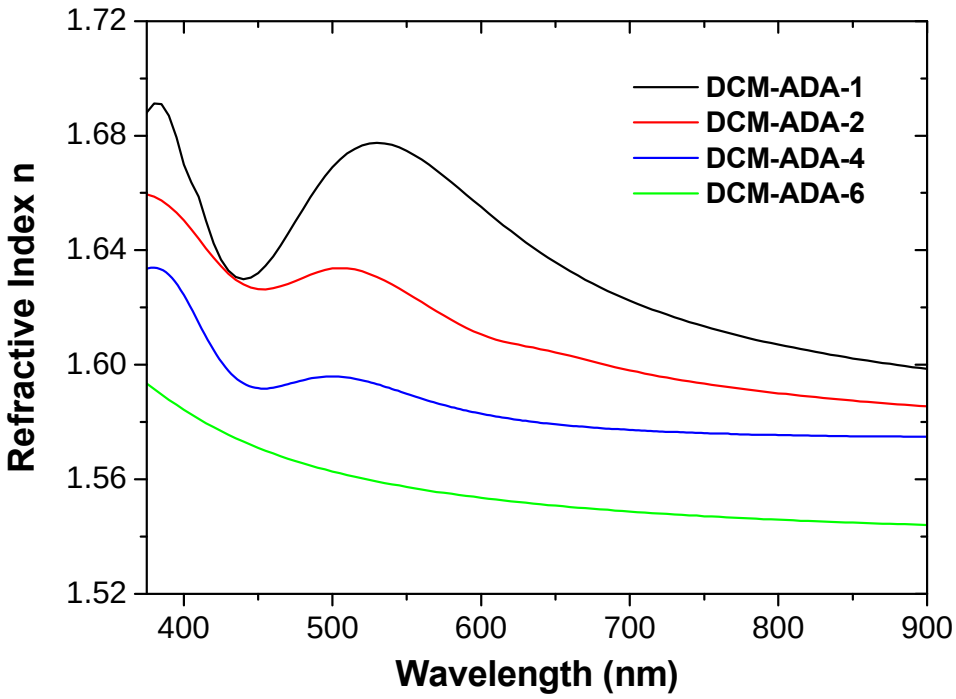

Figure 3. Refractive indices of selected samples as determined by variable angle spectroscopic ellipsometry. The samples were deposited on Si(100).

3.3 Steady-state and time-resolved luminescence

In addition to the deposition of stable colored plasma nanocomposites, our main objective involved using a laser dye such as DCM as a precursor is to fabricate luminescent films. Figure 4a shows the luminescence emission of the DCM-ADA films series when excited at 475 nm. The emission maxima of the films gradually shifted from ~638 nm for DCM-ADA-1 to ~547 nm for DCM-ADA-6. Thus, the emissions of the films were red-shifted as the DCM dye concentration in the film increased. These results contrast the transmission values in the previous section, where the shift in the absorption band as a function of the films' composition was almost negligible.

Vast literature exists that discusses the photophysical properties of DCM in solution. During the 1980s, Meyer and Mialocq analyzed the solvatochromic shift of both the absorption and fluorescence spectra of this dye for an ample range of solvents.[12] These authors found that the observed redshift of the emission band could be related to non-specific solute-solvent interactions.[36] Amongst the different models that have been proposed to explain the influence of the solvent's polarity on the photo-physical properties of organic dyes,[37] Meyer reported a clear correlation between the DCM Stokes shift and the Lipper-Mataga polarity function according to Eq. [1]:

$$\nu_A - \nu_F = \nu_{A-F} + \frac{2}{hca^3}\left(\mu_e - \mu_g\right)^2 \left(\frac{\varepsilon-1}{2\varepsilon+1} - \frac{n^2-1}{2n^2+1}\right) \quad [1]$$

where ν_A and ν_F are the absorption and emission frequencies, respectively; the constant $\nu_{A\text{-}F}$ is the Stokes shift in a vacuum (i.e., without solvent relaxation); h and c are Planck's constant and the speed of light, respectively; a is the radius of the spherical cavity in Onsager's theory of reaction fields, which in a first approximation can be calculated as half the long axis of the dye molecule; μ_e and μ_g are the excited- and ground-state dipole moments of the dye, respectively; and ε and n are the dielectric constant and refractive index of the solvent, respectively. [36]

In principle, we can reasonably assume that the gradual increase in the Stokes shift (cf. Figure 4) in our solid system could have been partially caused by an increase in the polarity of the plasma polymer-matrix that surrounded the dye. Thus, similar solid-state solvation effects have been reported for several DCM derivatives.[38,39] In our case, this effect might have been related to the higher presence of DCM fragments in the RPAVD films as the DCM/ADA sublimation ratio increased. The easiest method to confirm this point would be to analyze the Lippert-Mataga plot of these samples. However, the dielectric constant of these plasma polymer films is unknown.

Nonetheless, we could follow the same Lippert-Mataga formalism to obtain Eq. [2], which also relates the absorption and emission frequencies to the dielectric and refracting indices of the surrounding environment:

$$\nu_A + \nu_F = \nu_{A+F} - \frac{2}{hca^3}\left(\mu_e^2 - \mu_g^2\right)\left(\frac{\varepsilon-1}{2\varepsilon+1} + \frac{n^2-1}{2n^2+1}\right) \quad [2]$$

Here, we have a system of two linear equations in which the contacts ν_{A-F} and ν_{A+F} and the slopes $2(\mu_e-\mu_g)^2hca^{-3}$ and $2(\mu_e^2-\mu_g^2)hca^{-3}$ can be calculated by fitting the absorption and emission frequencies that have been reported in the literature for DCM in different solvents.[12]. Thus, if the evolution in the values of the Stokes shift in Figure 4 is exclusively caused by a non-specific solvatochromic effect, Eq. [2] should allow us to estimate the polarity function f(ε)+f(n) of the RPAVD samples, where f(x) = (x-1)/(2x+1). Figure S2 shows the $\nu_A+\nu_F$ vs. f(ε)+f(n) calibration curve, which was generated by using the information that was reported by Meyer. In this graph, we did not include those nonpolar solvents for which the Lippert-Mataga model is not valid, i.e., solvents 1-7 in reference 12. The f(ε)+f(n) polarity values of the RPAVD films were tentatively estimated according to the slope and intercept of the linear fit data in Figure S2 and the photo-physical properties of the RPAVD samples (i.e., the maxima of the emission and excitation peaks in cm^{-1}) (Table S1). The dielectric constant value for the DCM-ADA sample that was inferred from Table S1 ($\varepsilon \approx 3.2$) was similar to those that have been reported for other organic materials that were deposited by plasma methods,[40,41] while we obtained $\varepsilon \approx 11$ for the DCM sample, which was higher than the values that have been reported for high-k plasma polymers even in the case of hybrid systems.[42] Importantly, these values were calculated by considering that the photo-physical properties of the dye in the RPAVD samples were only affected by non-specific dye-media interactions and a model that was conceived for homogenous media. To

confirm this hypothesis, Figure 4c compares the Lippert-Mataga plots (Eq. [1]) of the RPAVD samples by using the f(ε)-f(n) values in Table S1 and the solutions that were analyzed by Meyer. For samples DCM-ADA-6 to 3, the Stokes shift and the estimated polarity function matched the linear evolution that was depicted by Meyer and the used Lippert-Mataga model. Therefore, the photo-physical properties of the films and the observed shift in the emission band for this first set of samples were mainly related to the stabilization of the excited state of the dipole moment of the DCM molecules in plasma polymer matrices of different polarity, similar to the phenomena in the diluted DCM solutions. Furthermore, this result validates the approach that was used to estimate the polarity function of the plasma matrix. In contrast, the remaining RPAVD samples strongly deviated from this trend in Figure 4, mainly for samples DCM-ADA-1 and DCM. This disagreement could have been caused by different factors. For instance, the FT-IR and UV-VIS spectra indicated that the DCM film, in contrast to the other samples, had a complex bound structure that mainly consisted of a high concentration of integer dye molecules in a solid matrix that was produced by the plasma fragmentation of the sublimated dye. This process might induce the development of specific large intermolecular interactions that are not considered in the Lippert-Mataga model.[36]

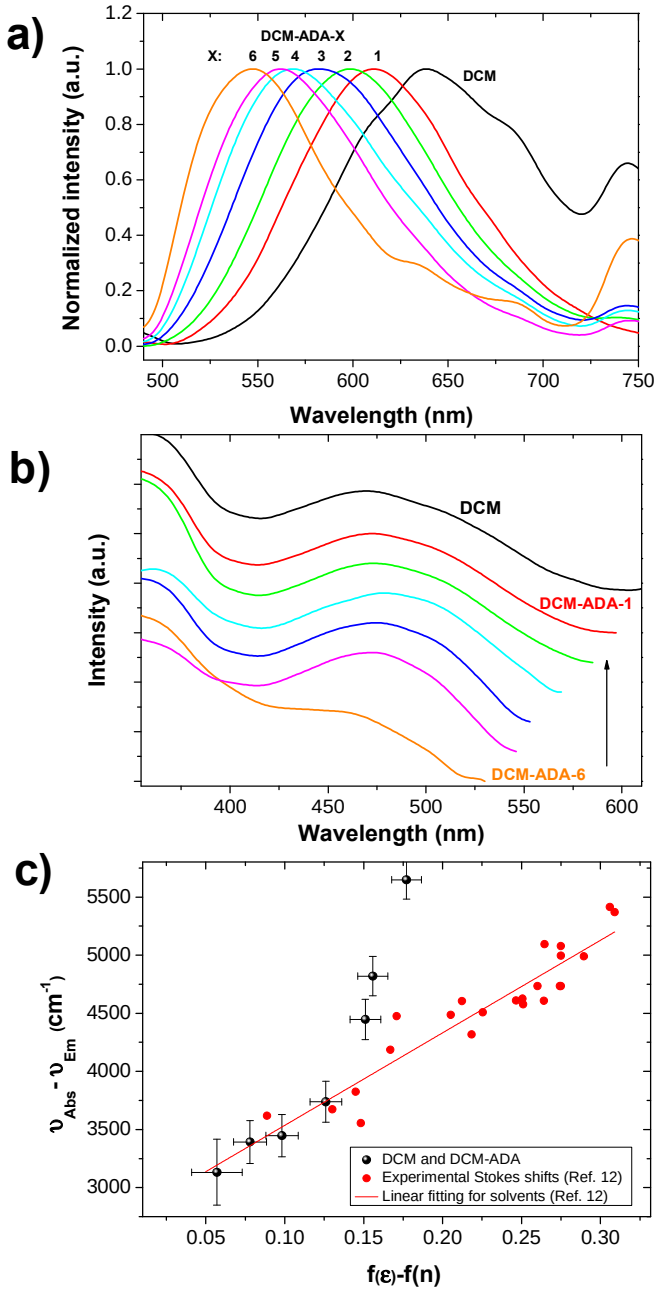

Figure 4. (a) Luminescent emissions of the DCM and DCM-ADA films when excited at 475 nm. (b) Excitation spectra of the DCM and DCM-ADA films. (c) Stokes shifts of the same samples versus the estimated Lippert-Mataga polarity function (black points). The red points correspond to the same curve for DCM in different solvents according to the data from reference 12. The red line corresponds to the linear fit of the latter set of data.

The gradual change in the emission color of ~100 nm as a function of the film's composition could be easily observed by visual inspection when the films were illuminated with a low-power UV source (λ= 365 nm) (see photograph in Figure 5a). The luminescent emission color defined the curve characteristic of this system in the CEI diagram (Figure 5a). This curve indicated the available colors through the DCM-ADA percentages were different from those in Table 1. Additionally, the curve determined the colors that could be obtained by producing multilayers or graded-composition DCM-ADA films, as shown in Figure 5b. Combining the deposition of these films enables us to designate the final emission of a composed film in the experimental emission range in Figure 4b by depositing a multilayer structure or gradually changing the experimental conditions during the film's deposition. An example of this approach is shown in Figure 4b, where a broad luminescent emission was obtained from a multilayer that consisted of DCM-ADA-5 and DCM-ADA-1, which were deposited sequentially in a ratio of 70:30.

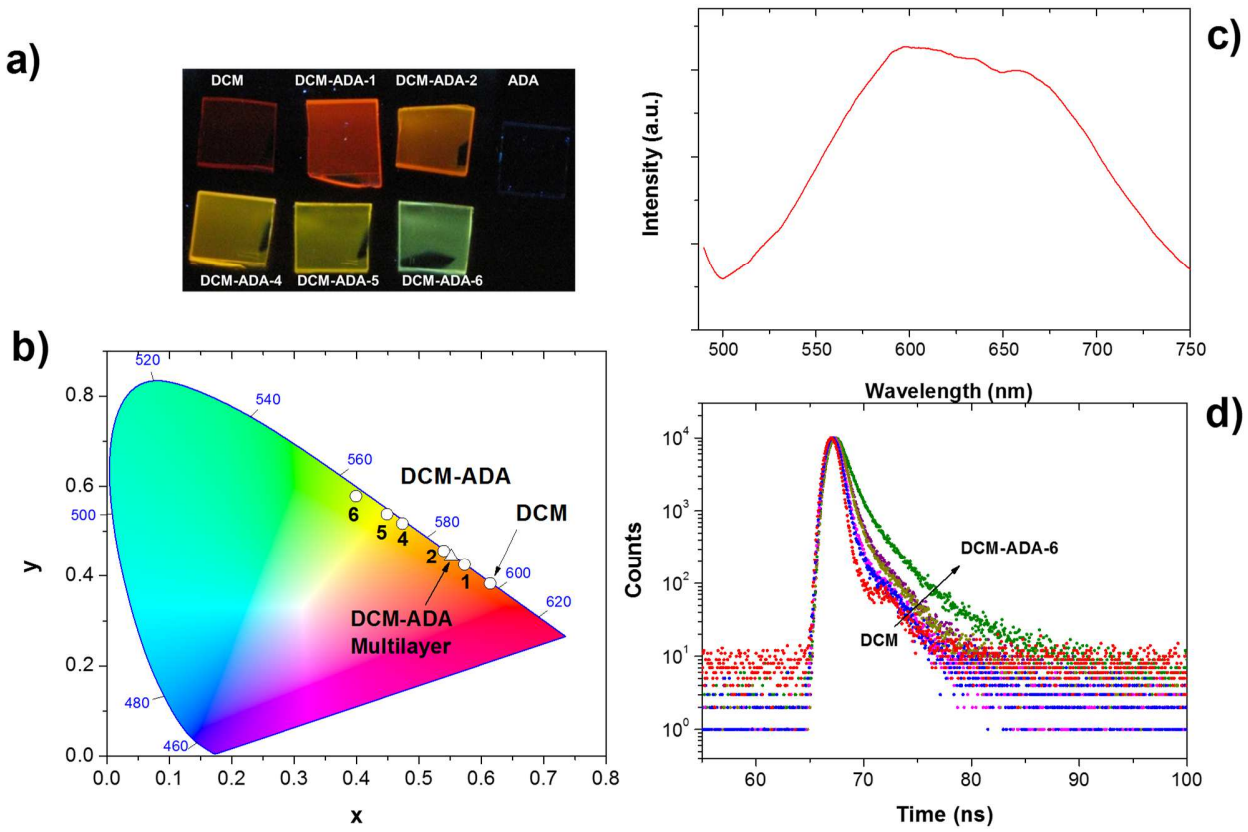

Figure 5. (a) Picture of the DCM and DCM-ADA films in Figure 3a when illuminated with a UV (365 nm) lamp. (b) CIE diagram that shows the luminescent color evolution of the ADA-DCM film series as a function of the films' composition. (c) Emission spectrum of a DCM-ADA multilayered film. (d) Luminescent decay curves at the DCM and DCM-ADA emission maxima when excited at 475 nm.

The experimental quantum yields for the studied films were 0.3% for the DCM film and 1.8%, 1.8%, 4.7%, 6.5% and 10.2% for the DCM-ADA-X films, where X=1, 2, 4, 5 and 6, respectively. Although these luminescent emissions could be observed by eye under ambient

light conditions, the quantum yield values were low but similar to those that have been reported for the direct DCM excitation in sublimated DCM blends with concentrations around 10%.[16]

Figure 5d shows the luminescent decay curves of the DCM-ADA film series' emissions when excited at 475 nm by using the nanosecond time-correlated single photon counting technique. Importantly, the excited ICT state is not populated by direct photoexcitation but is generated by an intramolecular charge transfer transition from a locally excited state. However, the characteristic time of this ultrafast process (typically in the range of fs) is shorter than the time resolution of our experimental set-up. The emission decay curves of the plasma nanocomposites cannot be adjusted to mono-exponential or bi-exponential functions, which require at least a tri-exponential model to obtain reliable fittings. Such complex multi-exponential decay curves are attributed to the different local environments where the dye molecules are trapped within the plasma polymeric matrix. In summary, the calculated decay models consisted of a very fast decay (τ< 1 ns) with a relative contribution higher than 80% and two slower components in the nanosecond range. The area under the decay curves in Figure 5 and, therefore, the calculated average lifetime gradually decreased with the DCM concentration from DMC-ADA-6 (τ_A = 1.4 ns) to DCM-ADA-1 (τ_A = 0.4 ns) and DCM (τ_A~ 0.2 ns), which indicates that the observed quantum yield reduction with the DCM concentration could be explained by an increase in the non-radiative deactivation processes that quenched the dye emission. As reported in the literature for this dye in other organic matrices, the reduction of the lifetime can be related to both concentration quenching[43] and an increase in the polarity of the host media, which was inferred from the previously discussed emission redshift.[13]

3.4 ASE experiments

In this section, we present a feasibility study regarding the possibilities of using DCM dye with plasma nanocomposites as gain media for lasing applications. Therefore, ASE experiments were performed on 700-nm-thick films that were deposited onto quartz substrates to assess if the DCM plasma nanocomposite films showed positive optical gain.

The measured refractive index of the quartz substrate (n= 1.45) was lower than that of the composite layers, as shown in Figure 3. The resulting quartz-polymer–air structure defined an asymmetric slab optical waveguide, where total internal reflection confined and guided the light along the film so that edge emission was achieved. The guided luminescence of the samples was detected through the edges of the films or scattered by the films' surface, but no difference was observed between any of the two detection geometries. The emission spectrum was recorded as a function of the pump power density for both the DCM and DCM-ADA composite films. For the DCM sample, a broad band spectrum that was similar to the black curve in the inset in Figure 6 was detected for the entire available pump power range. This result suggests that stimulated emission was not the main emission mechanism in this material despite the large pumping stripe, which should have lowered the ASE threshold.[34] Moreover, the fluorescence intensity irreversibly photobleached at moderate pump power densities (hundreds of kW/cm^2), whereas the thin films sublimated after a few pump pulses at the highest pump power, around 8 MW/cm^2. On the other hand, Figure 6a shows a narrow band at ~645 nm with a 15-nm full width at half maximum (FWHM) when pumped above a given power density, which is a clear signature of the ASE onset. Additionally, a 7-fold reduction occurred in the emission bandwidth threshold, which was comparable to the FWHM reductions in high-optical-gain organic materials.[23] The evolution of the FWHM of sample DCM-ADA-1 with the pump power density is given in Figure 6a.

Several methods exist to estimate the ASE threshold,[44] so we assumed here that the ASE threshold was the pump power at which the FWHM dropped to half its highest value. This threshold pump power coincided with that at which a change in slope occurred in the output intensity vs. pump power curve (not shown). The values for the DCM-ADA nanocomposite waveguides decreased as the dye concentration increased. Thus, the experimental ASE values for samples DCM-ADA-3, DCM-ADA-2, and DCM-ADA-1 were 860, 660 and 450 kW/cm^2, respectively. The best value, which corresponded to sample DCM-ADA-1, was of the same order of magnitude as that for Nile-blue dye-impregnated porous silica thin films (300 kW/cm^2)[45] and notably lower than that for Nile-blue doped PMMA polymer films (3 MW/cm^2).[46] However, samples of Sulforhodamine 640 that were doped in pHEMA films, which have emissions that are centered at 630 nm, rendered thresholds around 60 kW/cm^2, even under less favorable pumping conditions.[47] The reduced quantum yield of sample DCM-ADA-1 and the propagation losses of the waveguide from residual self-absorption in the DCM-ADA nanocomposite very likely increased the value of the ASE threshold in our system.

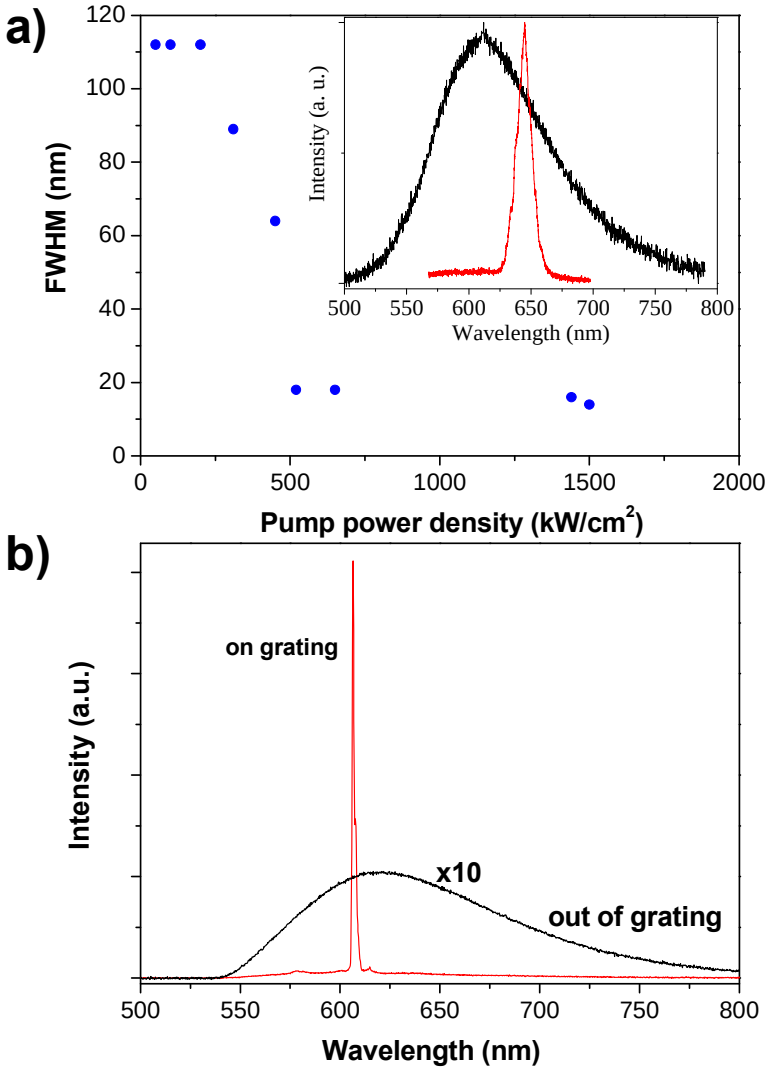

Figure 6. ASE experiments of a DCM-ADA-1 film on a quartz substrate. (a) FWHM of the emission band at different excitation power densities. The inset shows the normalized emission spectra of the DCM-ADA-1 composite waveguide above (red) and below (black) the ASE threshold. (b) DFB laser emission spectra of a DCM-ADA-1 film for a pump power of 2 MW/cm^2 when the excitation beam was focused on the grating area (red) and outside the grating area (black).

Furthermore, the emission intensity irreversibly photobleached after a few pump pulses above the ASE threshold. However, in contrast to the DCM films, the DCM-ADA nanocomposites did not sublimate even at the highest available pump power. This result demonstrates that the DCM-adamantane mixture provided a structure with improved mechanical properties and stability against external damage, such as photo-induced sublimation.

3.5 DFB laser experiments

Once we confirmed that thin DCM-ADA-1 films that were deposited by remote plasma polymerization showed positive optical gain, we proceeded to test this material for a DFB laser device. Therefore, a thin film of approximately 700-nm average thickness was deposited onto quartz substrates, with a 1D sinusoidal DFB structure engraved on the material with a period Λ=377 nm. This structure formed a 1D photonic crystal that could provide the necessary optical feedback to obtain laser emission at a wavelength that fulfilled the Bragg diffraction condition:

$$m\,\lambda_B = 2\,n_{eff}\,\Lambda \qquad (1)$$

where m is an integer that describes the order of the diffraction, λ_B is the wavelength of the stop-band (optical gap), Λ is the period of the 1D diffractive structure, and n_{eff} is the effective refractive index of the waveguide. n_{eff} depends on the refractive indices of the substrate, cladding (air) and deposited layer and on the film's thickness. For the second diffraction order (m = 2), the resonant light wavelength equals $n_{eff}\Lambda$ and is diffracted out of the surface of the film perpendicular to the plane of the waveguide.[17] The characteristic broad emission band of the DCM-ADA-1 fluorescence was recorded when the waveguide was excited outside the 1D photonic structure at a pump power of approximately 2 MW/cm^2, well above the laser threshold (see below), as shown in Figure 6b. However, a very narrow (0.6-nm FWHM) and intense

emission line that was centered at 607 nm was detected when the excitation beam was shifted to the 1D corrugated area, which was associated with DFB laser emission (see the sharp red peak in Figure 6b. A 700-nm-thick waveguide with a refractive index of 1.65 at 607 nm that was deposited onto a quartz substrate (n = 1.456) exhibited 4 guided modes, specifically, 2 transverse electric (TE_0 and TE_1, n_{eff}=1.635 and 1.531, respectively) and 2 transverse magnetic modes (TM_0 and TM_1, n_{eff}=1.628 and 1.511, respectively). Substituting the emission wavelength and grating period Λ= 377 nm into the Bragg condition ($\lambda_B = n_{eff}\,\Lambda$) rendered an effective index n_{eff}~1.61, which was close to the effective indices of the TE_0 and TM_0 modes. Thus, the oscillating mode in our device would correspond to one of these modes. The polarization measurements, which are shown below, would help to discriminate between these modes. On the other hand, the spectral width of the laser emission probably formed from heterogeneities in both the film's thickness and the photonic structure's groove separation along the pumped area, which implies variations in n_{eff} and, in turn, the resonant wavelength.

Further evidence of the DFB laser was obtained by studying the emissions as a function of the pump power. An abrupt increase in the emission intensity at 607 nm, followed by a linear dependence on the pump power (Figure 7a) and a sharp spectral narrowing (Figure 7b), were observed at a pump power density of 380 kW/cm^2, which corresponded to the DFB laser threshold. The relatively large value of the DFB laser threshold was attributed to self-absorption losses at the tail of the absorption band at 607 nm. Below the laser threshold, the emission spectrum consisted of three peaks that were separated by two dips (Figure 7b). These dips corresponded to stop-bands that were forced in the waveguide modes by the 1D photonic structure. Above the pump threshold, DFB laser oscillation occurred at the long-wavelength edge of the photonic forbidden band, where the density of the permitted photon states was highest and

the output coupling losses were lowest (Figure 7b).[21,47] The positions of the stop-bands in the photonic lattice depended on the propagation direction. In particular, a redshift in the stop-band was expected when changing the detection angle in the incident plane below the pump threshold. This effect is evidenced in Figure 7c, where the emission spectra for a pump power below the laser threshold showed that the stop-bands shifted to longer wavelengths as the detection angle changed from the normal direction. Nevertheless, the DFB laser emission above the pump threshold was strongly directional (perpendicular to the surface) and did not change its emission wavelength when changing the detection angle. Indeed, no laser emission was detected at an angle slightly higher than 1.5º from the normal direction (Figure 7d).

The polarization dependence was studied to complete the characterization of the DFB laser emission. DFB laser emission from the thin polymer film was observed when the polarization of the excitation beam was parallel to the grating grooves, while no laser emission was induced at any available pump power when the excitation polarization was perpendicular to the grating lines. A similar behavior has been observed before[48] and is ascribed to the degree of overlapping between the grating wave vector (which is perpendicular to the grooves and parallel to the structure) and the transition dipole moment of the emitting molecule. In this sense, the more perpendicular these vectors are, the lower the threshold becomes. Moreover, the polarization of the DFB laser was found to be linear and parallel to the grating grooves. This last result clearly indicates that the light in our DFB structure was oscillating in the fundamental TE_0 mode because the electric field was propagated parallel to the grooves; thus, when the light was out-coupled from the waveguide, its polarization was maintained in this orientation. On the contrary, if the TM_0 mode had oscillated, the electric field would have been arranged in a plane that was perpendicular to the grooves and would have been out-coupled in this direction. According to

these results, the absorption and emission transition dipole moments in the DCM-adamantane nanocomposite were mostly parallel.

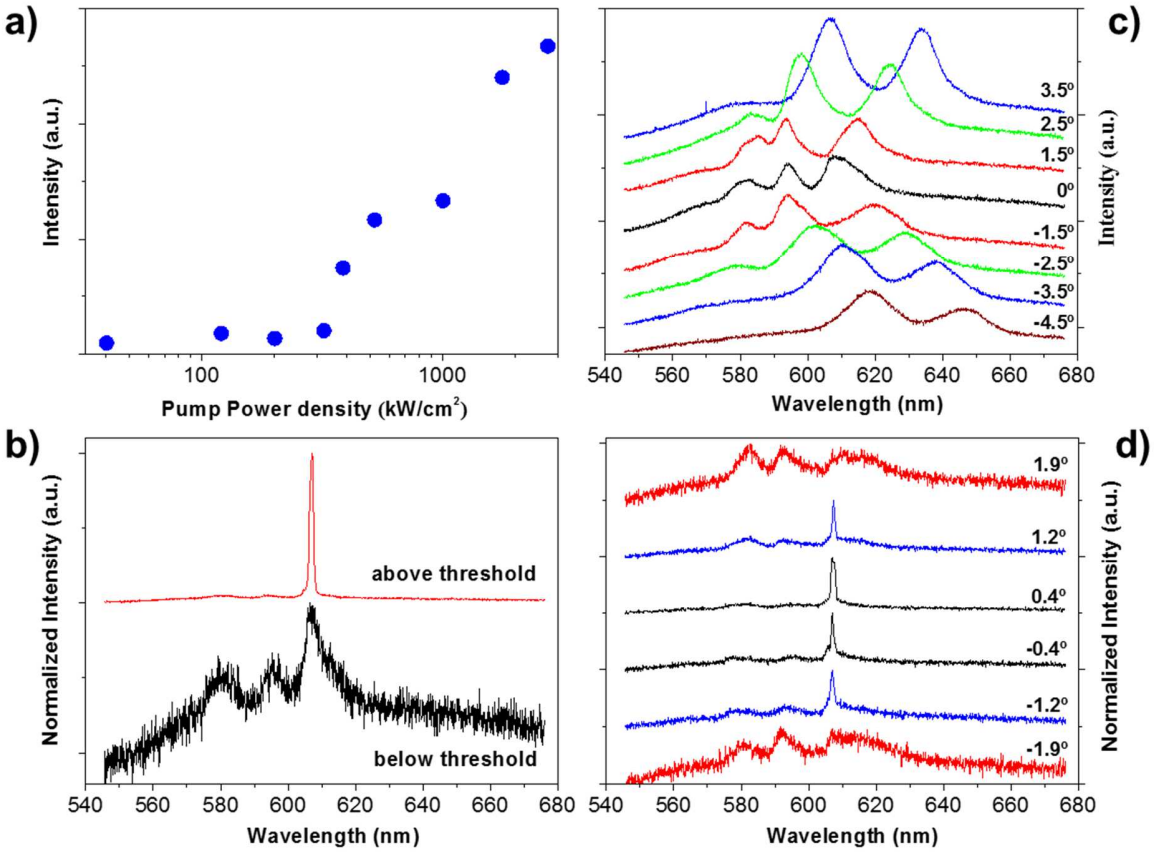

Figure 7. (a) Output emission intensity of the DCM-ADA DFB laser as a function of the pump power. (b) Normalized emission spectra that was measured normal to the surface above (red) and below (black) the laser threshold. (c) Angular dependence of the photonic stop-bands for a pump power below the laser threshold. The detection angle that was used with respect to the normal is given. (d) Angular dependence of the DFB laser emission. The detection angle with respect to the normal is given. The pump power was above the laser threshold, and the spectra were normalized for clarity.

4. CONCLUSIONS

In this work, we presented the remote plasma-assisted vacuum deposition of nanocomposite thin films with an adamantane solid precursor and the DCM laser dye. The obtained films were thermally and chemically stable at temperatures even higher than those that correspond to the precursor's sublimation. The films presented good optical quality, with refractive indices that were tunable over a relatively wide range. Thus, the ADA films showed a relatively high refractive index, and even higher values (up to 1.67 at 550 nm) were determined as the dye percentage in the film increased. These results indicated that luminescent emission was also a function of the concentration of integer and fragmented dye molecules in the matrix, showing increments in the quantum efficiency and shift to lower wavelengths as the dilution increased. Thus, the absorption spectra of the films only significantly differed in their color intensity, but the corresponding stoke shifts varied by up to 100 nm between the lower and higher dye concentrations, which was attributed to differences in the polarity of the local environment surrounding the DCM emitters in the films. We demonstrated that DCM-adamantane nanocomposite films showed improved stability against photo-induced sublimation compared to plasma DCM films. Moreover, ASE experiments showed positive optical gain, with a threshold of 450 kW/cm^2 in the nanocomposite material, while no ASE was detected in the DCM waveguides. In addition, DFB laser emission was observed when the thin remote plasma polymerization composite dye film was deposited on a 1D corrugated silica substrate. The DFB laser emission was directional and linearly polarized parallel to the grating lines and had a threshold of 380 kW/cm^2.

These results introduced lasing in films that were deposited by remote plasma-assisted vacuum deposition. Additional studies are required to optimize the luminescence efficiencies of these

nanocomposite films. For example, the use of derivative DCM dye precursors to avoid intermolecular interactions at high concentrations[39] or Förster energy transfer to the DCM from an acceptor dye[16,38] are feasible strategies to improve the photoluminescence of the films and reduce the lasing thresholds. However, these results clearly show the available synthetic approaches to control properties such as light absorption, fluorescence and the refractive index, which are critical to designing optically active thin films by the remote plasma-assisted technique. These results will find significant applications in optoelectronics, integrated photonics and the design of functional coatings.

ASSOCIATED CONTENT

Supporting Information. The ToF-SIMS analysis of the luminescent nanocomposite films (S1) and complimentary data concerning the polarity characterization of the DCM-ADA system (Figure S2 and Table S1) are available free of charge via the Internet at http://pubs.acs.org.

AUTHOR INFORMATION

Corresponding Authors' E-mail: fjaparicio@icmse.csic.es, angel.barranco@csic.es

Author Contributions

This manuscript was written through contributions of all the authors. All the authors have approved the final version of the manuscript.

ACKNOWLEDGMENTS

The authors thank the European Regional Development Funds program (EU-FEDER), the Junta de Andalucía (TEP8067) and the Spanish Ministry of Economy and Competitiveness (Projects MAT2016-79866-R, MAT2013-40852-R, MAT2013-42900-P, MAT2014-51937-C3-1-P,

RECUPERA 2020 and IJCI-2014-21260) for their financial support. We also thank Carmen Serra from CACTI (Universidad de Vigo) and F. Yubero (ICMS-CSIC) for their support during the ToF-SIMS and optical characterizations, respectively.

REFERENCES

(1) Ostrikov, K.; Neyts, E.C.; Meyyappan, M. Plasma Nanoscience: from Nano-Solids in Plasmas to Nano-Plasmas in Solids. *Adv. Phys.* **2013**, 62, 113-224.

(2) Ostrikov, K.; Cvelbar, U.; Murphy, A.B. Plasma Nanoscience: Setting Directions, Tackling Grand Challenges. *J. Appl. Phys. D* **2011**, 44, 174001.

(3) Aparicio, F. J.; Alcaire, M.; Borras, A.; Gonzalez, J. C.; Lopez-Arbeloa, F.; Blaszczyk-Lezak, I.; Gonzalez-Elipe, A. R.; Barranco, A. Luminescent 3-Hydroxyflavone Nanocomposites with a Tuneable Refractive Index for Photonics and UV Detection by Plasma Assisted Vacuum Deposition. *J. Phys. Chem. C* **2014,** 2, 6561-6573.

(4) Aparicio, F. J.; Blaszczyk-Lezak, I.; Sanchez-Valencia, J. R.; Alcaire, M.; Gonzalez, J. C.; Serra, C.; Gonzalez-Elipe, A. R.; Barranco, A. Plasma Deposition of Perylene-Adamantane Nanocomposite Thin Films for NO_2 Room-Temperature Optical Sensing. *J. Phys. Chem. C* **2012**, 116, (15), 8731-8740.

(5) Aparicio, F. J.; Holgado, M.; Borras, A.; Blaszczyk-Lezak, I.; Griol, A.; Barrios, C. A.; Casquel, R.; Sanza, F. J.; Sohlstrom, H.; Antelius, M.; Gonzalez-Elipe, A. R.; Barranco, A. Transparent Nanometric Organic Luminescent Films as UV-Active Components in Photonic Structures. *Adv. Mater.* **2011**, 23, 761-765.

(6) Aparicio, F.J.; Alcaire, M.; González-Elipe, A.R.; Barranco, A.; Holgado, M.; Casquel, R.; Sanza, F.J.; Griol, A.; Bernier, D.; Dortu, F.; Cáceres, S.; Antelius, M.; Lapisa, M.; Sohlström, H., Niklaus, F. Dye-Based Photonic Sensing Systems. *Sens. Actuators, B* **2016**, 228, 649-657.

(7) Barranco, A.; Groening, P. Fluorescent Plasma Nanocomposite Thin Films Containing Nonaggregated Rhodamine 6G Laser Dye Molecules. *Langmuir* **2006**, 22, 6719-6722.

(8) Webster, F. G.; McColgin, W. M. Arylidene Dye Lasers. US Patent nº US3852683 A, 1974.

(9) Meyer, M.; Mialocq, J. C.; Rougée, M. Fluorescence Lifetime Measurements of the Two Isomers of the Laser Dye DCM. *Chem. Phys. Lett.* **1988**, 150, 484-490.

(10) Hammond, P. R. Laser Dye DCM, its Spectral Properties, Synthesis and Comparison with other Dyes in the Red. *Opt. Commun.* **1979**, 29, 331-333.

(11) Marason, E. G. Laser dye DCM: CW, Synchronously Pumped, Cavity Pumped and Single-Frequency Performance. *Opt. Commun.* **1981**, 37, 56-58.

(12) Meyer, M.; Mialocq, J.C. Ground State and Singlet Excited State of Laser Dye DCM: Dipole Moments and Solvent Induced Spectral Shifts. *Opt. Commun*. **1987**, 64, 264-268.

(13) Kwak, G.; Okada, C.; Fujiki, M.; Takeda, H.; Nishida, T.; Shiosaki, T. Polar Laser Dyes Dispersed in Polymer Matrices: Reverification of Charge Transfer Character and New Optical Functions. *Jpn. J. Appl. Phys.* **2008**, 47, 1753-1756.

(14) Kaur, A.; Cazeca, M. J.; Sengupta, S. K.; Kumar, J.; Tripathy, S. K. Voltage Tunable Multicolor Light Emitting Diodes Based on a Dye-Doped Polythiophene Derivative. *Synth. Met.* **2002**, 126, 283-288.

(15) Guo, Z.; Zhu, W.; Tian, H. Dicyanomethylene-4H-pyran Chromophores for OLED Emitters, Logic Gates and Optical Chemosensors. *Chem. Commun.* **2012**, 48, 6073-6084.

(16) Toffanin, S.; Capelli, R.; Hwu, T.-Y.; Wong, K.-T.; Plötzing, T.; Först, M.; Muccini, M. Molecular Host−Guest Energy-Transfer System with an Ultralow Amplified Spontaneous Emission Threshold Employing an Ambipolar Semiconducting Host Matrix. *J. Phys. Chem. B* **2009**, 114, 120-127.

(17) Qin, W.; Ding, D.; Liu, J.; Yuan, W. Z.; Hu, Y.; Liu, B.; Tang, B. Z. Biocompatible Nanoparticles with Aggregation-Induced Emission Characteristics as Far-Red/Near-Infrared Fluorescent Bioprobes for In Vitro and In Vivo Imaging Applications. *Adv. Funct. Mater.* **2012**, 22, 771-779.

(18) Cheon, C. H.; Joo, S.-H.; Kim, K.; Jin, J.-I.; Shin, H.-W.; Kim, Y.-R. Synthesis and Luminescent Properties of Fluorene Copolymers Bearing DCM Pendants. *Macromolecules* **2005**, 38, 6336-6345.

(19) Barranco, A.; Cotrino, J.; Yubero, F.; Girardeau, T.; Camelio, S.; González-Elipe, A. R. A Structural Study of Organo-Silicon Polymeric Thin Films Deposited by Remote Microwave Plasma Enhanced Chemical Vapour Deposition. *Surf. Coat. Tech.* **2004**, 180–181, 244-249.

(20) Siegman, A. E. *Lasers*; University Science Books: Mill Valey, CA, 1986.

(21) Samuel, I. D. W.; Turnbull, G. A. Organic Semiconductor Lasers. *Chem. Rev.* **2007**, 107, 1272-1295.

(22) Grivas, C.; Pollnau, M. Organic Solid-State Integrated Amplifiers and Lasers. *Laser Phot. Rev.* **2012**, 6, 419-462.

(23) Calzado, E. M.; Boj, P. G.; Díaz-García, M. A. Amplified Spontaneous Emission Properties of Semiconducting Organic Materials. *Int. J. Mol. Sci.* **2010**, 11, 2546-2565.

(24) Costela, A.; García, O.; Cerdán, L.; García-Moreno, I.; Sastre, R. Amplified Spontaneous Emission and Optical Gain Measurements from Pyrromethene 567-Doped Polymer Waveguides and Quasi-Waveguides. *Opt. Express* **2008**, 16, 7023-7036.

(25) Yang, P. D.; Wirnsberger, G.; Huang, H. C.; Cordero, S. R.; McGehee, M. D.; Scott, B.; Deng, T.; Whitesides, G. M.; Chmelka, B. F.; Buratto, S. K.; Stucky, G. D. Mirrorless Lasing From Mesostructured Waveguides Patterned by Soft Lithography. *Science* **2000**, 287, 465-467.

(26) Cerdán, L.; Costela, A.; Duran-Sampedro, G.; Garcia-Moreno, I. Random Lasing From Sulforhodamine Dye-Doped Polymer Films with High Surface Roughness. *Appl. Phys. B.* **2012**, 108, 839-850.

(27) Blaszczyk-Lezak, I.; Aparicio, F. J.; Borras, A.; Barranco, A.; Alvarez-Herrero, A.; Fernandez-Rodriguez, M.; Gonzalez-Elipe, A. R. Optically Active Luminescent Perylene Thin Films Deposited by Plasma Polymerization. *J. Phys. Chem. C* **2009**, 113, 431-438.

(28) Briggs D.,; Seah, M. P. *Applications of XPS in Polymer Technology in Practical Surface Analysis*. Second ed.; John Wiley & Sons Ltd: Chichester, 1990, pp 437-484.

(29) Ferrer, F. J.; Alcaire, M.; Caballero-Hernández, J.; Garcia-Garcia, F. J.; Gil-Rostra, J.; Terriza, A.; Godinho, V.; García-López, J.; Barranco, A.; Fernández-Camacho, A. Simultaneous Quantification of Light Elements in Thin Films Deposited on Si Substrates Using Proton EBS (Elastic Backscattering Spectroscopy). *Nucl. Instrum. Methods Phys. Res., Sect. B* **2014**, 332, 449-453.

(30) D'Agostino, R., Ed. *Plasma Deposition, Treatment, and Etching of Polymers*; Academic Press Inc: San Diego, CA, 1990.

(31) Aparicio, F. J.; Borras, A.; Blaszczyk-Lezak, I.; Groning, P.; Alvarez-Herrero, A.; Fernandez-Rodriguez, M.; Gonzalez-Elipe, A. R.; Barranco, A. Luminescent and Optical Properties of Nanocomposite Thin Films Deposited by Remote Plasma Polymerization of Rhodamine 6G. *Plasma Processes Polym.* **2009**, 6, 17-26.

(32) Jiang, H., Grant, J. T., Enlow, J., Suae, W., Bunning, T. J. Surface Oxygen in Plasma Polymerized Films. *J. Mater. Chem.* **2009**, 19, 2234-2239.

(33) Sokrates, G. *Infrared Characteristic Group Frequencies: Tables and Charts*; Wiley-Interscience: New York, NY, 1994.

(34) Tassle, A. J. V., Prantil, M. A., Fleming, G. R. Investigation of the Excited State Structure of DCM via Ultrafast Electronic Pump/Vibrational Probe. *J. Phys. Chem. B* **2006**, 110, 18989–18995.

(35) Martinu, L.; Poitras, D. Plasma Deposition of Optical Films and Coatings: A Review. *J. Vac. Sci. Technol., A* **2000**, 18, 2619-2645.

(36) Lakowicz, J. R., *Principles of Fluorescence Spectroscopy*, 3rd ed; Springer: New York (NY), 2006; Chapter 6, pp 205-235.

(37) Kawski, A. On the Estimation of Excited-State Dipole Moments from Solvatochromic Shifts of Absorption and Fluorescence Spectra. *Z. Naturforsch.* **2002**, 57a, 255–262.

(38) Vembris, A.; Zarins, E.; Kokars, V. Solid State Solvation Effect and Reduced Amplified Spontaneous Emission Threshold Value of Glass Forming DCM Derivative in PMMA films. *J. Lumin*. **2015**, 158, 441-446.

(39) Kozlov, V. G.; Bulovic, V.; Burrows, P. E.; Baldo, M.; Khalfin, V. B.; Parthasarathy, G.; Forrest, S. R.; You, Y.; Thompson, M. E. Study of Lasing Action Based on Förster Energy Transfer in Optically Pumped Organic Semiconductor Thin Films. *J. Appl. Phys.* **1998**, 84, 4096-4108.

(40) Kim, M. C.; Cho, S. H.; Lee, S. B.; Kim Y.; Boo, J. H. Characterization of Polymer-Like Thin Films Deposited on Silicon and Glass Substrates Using PECVD Method. *Thin Solid Films* **2004**, 447–448, 592-598.

(41) Xu Y.; Berger, P. R.; Cho, J.; Timmons, R. B. Capacitance-Voltage Characterization of Pulsed Plasma Polymerized Allylamine Dielectrics for Flexible Polymeric Field Effect Transistors. *J. Electron. Mater*. **2004**, 33, 1240-1247.

(42) Yu, Y. –Y.; Jiang, A.-H; Lee, W.-Y. Organic/Inorganic Nano-Hybrids with High Dielectric Constant for Organic Thin Film Transistor Applications. *Nanoscale Res. Lett.* **2016**, 11, 488.

(43) Green, A. P.; Buckely, A. R. Solid State Concentration Quenching of Organic Fluorophores in PMMA. *Phys. Chem. Chem. Phys.* **2015**, 17, 1435-1440.

(44) Cerdán, L.; Costela, A.; García-Moreno, I. On the Characteristic Lengths in the Variable Stripe Length Method for Optical Gain Measurements. *J. Opt. Soc. Am. B* **2010**, 27, 1874-1877.

(45) Oton, C. J.; Navarro-Urrios, D.; Capuj, N. E.; Ghulinyan, M.; Pavesi, L.; González-Pérez, S.; Lahoz, F.; Martín, I. R., Optical Gain in Dye-Impregnated Oxidized Porous Silicon Waveguides. *Appl. Phys. Lett.* **2006**, 89, 011107.

(46) Navarro-Urrios, D.; Ghulinyan, M.; Bettotti, P.; Rigo, E.; Oton, C. J.; Capuj, N. E.; Lahoz, F.; Martín, I. R.; Pavesi, L. Polymeric Waveguides Using Oxidized Porous Silicon Cladding for Optical Amplification. *Opt. Mater.* **2009**, 31, 1488-1491.

(47) Turnbull, G. A.; Andrew, P.; Barnes, W. L.; Samuel, I. D. W. Operating Characteristics of a Semiconducting Polymer Laser Pumped by a Microchip Laser. *Appl. Phys. Lett.* **2003**, 82, 313-315.

(48) Wright, D.; Brasselet, E.; Zyss, J.; Langer, G.; Kern, W. Dye-Doped Organic Distributed-Feedback Lasers with Index and Surface Gratings: the Role of Pump Polarization and Molecular Orientation. *J. Opt. Soc. Am. B.* **2004**, 21, 944-950.

Table of content